Robotica: (2019) volume 37, pp. 1785–1803. © Cambridge University Press 2019
doi:10.1017/S0263574719000262

Design Boundary Layer Thickness and Switching Gain in SMC Algorithm for AUV Motion Control

Ehsan Taheri†*, Mohamad Hossein Ferdowsi† and Mohammad Danesh‡

†*Control Group, Electrical Engineering Department, Malek Ashtar University of Technology, 15875-1774, Tehran, Iran*
‡*Department of Mechanical Engineering, Isfahan University of Technology, 84156-83111, Isfahan, Iran*

(Accepted February 13, 2019. First published online: March 20, 2019)

SUMMARY
Designing the boundary layer thickness and switching gain in the nonlinear part of sliding mode controller (SMC) is one of the main subjects in SMC design that needs human experience, knowledge on the amplitude of disturbances, and information about the bounds of system uncertainties. In this paper, to reduce the trial-and-error effort by the designer(s) two different fitness functions in the horizontal and vertical planes are presented and a heuristic method is used for their optimization. The optimal switching gain in the proposed approach properly compensates the unmodeled dynamics, model uncertainty, and external disturbances. Chattering phenomenon in control signals and noise measurement effect are reduced by the optimal selection of boundary layer thickness. This proposed method is applied to an autonomous underwater vehicle (AUV) and evaluated through the real-time and cost-effective manner. The execution code is implemented on a single-board computer (SBC) through the xPC Target and is evaluated by the processor-in-the-loop (PIL) test. The results of the PIL test in the two different test cases indicate that the chattering phenomenon and amplitude of control signal applied to the actuators are reduced in comparison with the three conventional approaches in the AUV motion control.

KEYWORDS: Processor-in-the-loop test; Sliding mode controller; Autonomous underwater vehicle; Heuristic optimization algorithm.

1. Introduction

AUV performances in marine science, commercial, and military operations have increased over the past two decades, thus, the necessity for more studies to be run in this field. One of the critical bottlenecks in developing autonomous underwater vehicles (AUVs) is the technology readiness level (TRL) in the motion control area. Motion control algorithm design for AUVs is a hard task for the following reasons: limited amount of force, torque, velocity and acceleration, its inherent nonlinear dynamics, structured and unstructured uncertainties, external disturbances, time-varying parameters, time-varying environment, shallow water effect, coupling between the degrees of freedom (DOFs), and limited number of actuators with respect to the DOFs (under actuator constraints). Consequently, the above-mentioned reasons must be of concern during the development of motion control algorithms for AUVs. To accomplish motion control of an under-actuated robot, many attempts are made with respect to the limited number of actuators in comparison with DOFs. Detailed analysis is run to

* Corresponding author. E-mail: taheri.ehsan@mut-es.ac.ir

describe the current state of the art of motion control and path planning issues in.[1,2] In Cue et al.,[3] a complete study is presented about the integral sliding mode controller (SMC) through the multiple-input and multiple-output extended-state-observer (MIMO-ESO) for marine robotics. In this paper, an adaptive MIMO-ESO is proposed to estimate the unmeasured parameters and the unknown external disturbances. By considering specific constraints in the sliding-mode-based adaptive control, the AUV attitude control is designed.[4] This controller is combined with a nonlinear disturbance observer; the effectiveness of which is evaluated through the experimental results. To obtain an optimal path tracking for an AUV, a reinforcement learning algorithm is integrated with two neural networks in Cui et al.[5] For AUV flight control, different control algorithms have been and are being developed such as robust H∞ controller,[6,7] LQR,[8,9] PID control,[10,11] μ synthesis,[12] backstepping,[13,14] SMC,[15–17] self-tuning,[18,19] adaptive,[20] gain scheduling,[21] model predictive,[22] soft computing,[23,24] hybrid controller,[25] etc. Each of these motion control algorithms has its own advantages and disadvantages. Among the most controllers mentioned above, robust control methods are popular in AUV flight control because they can counteract uncertainty and external disturbances. Variable structure control (VSC) is a robust control, the variable structure of, which allows it to obtain the desired performance during closed-loop control process. SMC is the most well-known VSC. The basic idea of SMC was introduced by Utkin[15] which was applied to a marine vehicle by Yoerger and Slotine[16] for the first time. SMC as other control methods has its advantages of high robustness against uncertainties and disturbances, and disadvantages of chattering phenomenon due to the discontinuity in the control law. Due to high robustness against uncertainties/disturbances, SMC has been and is being widely combined with other methods to obtain better results in both theoretical research and practical engineering.

In this study, an SMC with optimal parameters in the nonlinear part of the controller is proposed through a heuristic optimization algorithm for controlling an AUV. The main contributions of this paper are summarized as follows:

- The boundary layer thickness in the nonlinear part of the control law is designed through two different fitness functions in the horizontal and vertical planes which are optimized through a heuristic algorithm. The proposed approach does not need human experience, knowledge on disturbances amplitude, and information on the bounds of system uncertainties. Therefore, trial-and-error efforts are reduced by the designer(s). Here, chattering phenomenon in control signals and noise measurement effect are reduced by the optimal selection of boundary layer thickness.
- The switching gain in the nonlinear part of the control law is optimally designed to compensate the unmodeled dynamics, model uncertainty, and external disturbances in an appropriate manner.
- The performance of this algorithm in the presence of external disturbances and model uncertainties is evaluated in the AUV motion control through the real-time PIL test by using the xPC Target. In this test, host PC is Axiomtek SBC 84710 which is used as the high-level processor in the actual AUV. In this manner, before the actual AUV becomes involved in factory acceptance tests (FAT), harbor acceptance tests (HAT), and sea acceptance tests (SAT), the execution codes are debugged and verified in a cost-effective manner, which in turn reduce the risks thereof.

The remainder of this paper is organized as follows. A brief background of a mathematical dynamic model for the AUV and conventional AUV motion control algorithms is described in Section 2. The proposed method is presented and implemented through the xPC Target on an SBC for evaluating through the PIL test in Section 3. The performance and effectiveness of the proposed method are demonstrated and compared with three conventional approaches in the AUV motion control by two different test cases with special maneuvers in 3D space in Section 4. Finally, the article is concluded in Section 5.

2. AUV Dynamic and Conventional Control

2.1. Coordinate systems

All six DOFs are required to fully describe the position and orientation of the AUV in a 3D space. The first three components and their time-derivatives through the transformation matrix describe the position and the linear velocity of the AUV, respectively. The second three components and their

https://doi.org/10.1017/S0263574719000262 Published online by Cambridge University Press

Table I. Symbols in the AUV dynamic model.

DOF	Describing the parameters	Forces and moments	Linear and angular velocities	Positions and Euler angles
1	Surge	X	u	x
2	Sway	Y	v	y
3	Heave	Z	w	z
4	Roll	K	p	ϕ
5	Pitch	M	q	θ
6	Yaw	N	r	ψ

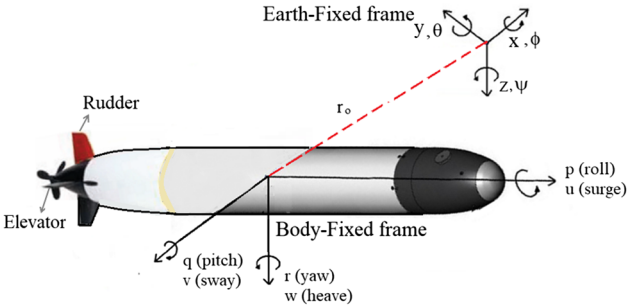

Fig. 1. Body and Inertia reference frames.

time-derivatives through the transformation matrix describe the orientation and the angular velocities of the AUV, respectively. The description of each of these six components is presented in Fig. 1 and Table I.

Due to the low-speed motion of the AUV, earth's motion can be neglected; hence, a point on the surface of the earth can be assumed to be fixed and applied as the center of the inertial coordinate system.

2.2. *Kinematic equations of motion*

The kinematic motion equations for an AUV, which deals with the geometric aspects of motion, are expressed in a general form as follows:

$$\begin{aligned} &\dot{\eta} = J(\eta)\nu \leftrightarrow \begin{bmatrix} \dot{\eta}_1 \\ \dot{\eta}_2 \end{bmatrix} = \begin{bmatrix} J_1(\eta_2) & 0_{3\times 3} \\ 0_{3\times 3} & J_2(\eta_2) \end{bmatrix} \begin{bmatrix} \nu_1 \\ \nu_2 \end{bmatrix}, \\ &\eta = \left[\eta_1^T, \eta_2^T\right]^T, \quad \eta_1 = [x\ y\ z]^T, \quad \eta_2 = [\phi\ \theta\ \psi]^T, \\ &\nu = \left[\nu_1^T, \nu_2^T\right]^T, \quad \nu_1 = [u\ v\ w]^T, \quad \nu_2 = [p\ q\ r]^T \end{aligned} \tag{1}$$

where the vector $\eta \in R^6$shows the position and orientation of the AUV with respect to the earth-fixed frame, $\nu \in R^6$ is a linear and angular velocities vector in the body-fixed frame, and $J : R^6 \to R^{6\times 6}$ is the transformation matrix relating the two frames. $J_1(\eta_2) = C_{z.\psi}^T C_{y.\theta}^T C_{x.\phi}^T$ describes the correlation between the position and linear velocities:

$$\begin{bmatrix} \dot{x} \\ \dot{y} \\ \dot{z} \end{bmatrix} = J_1(\eta_2) \begin{bmatrix} u \\ v \\ w \end{bmatrix}, \quad C_{z.\psi}^T = \begin{bmatrix} \cos\psi & -\sin\psi & 0 \\ \sin\psi & \cos\psi & 0 \\ 0 & 0 & 1 \end{bmatrix},$$

$$C_{y.\theta}^T = \begin{bmatrix} \cos\theta & 0 & \sin\theta \\ 0 & 1 & 0 \\ -\sin\theta & 0 & \cos\theta \end{bmatrix}, \quad C_{x.\phi}^T = \begin{bmatrix} 1 & 0 & 0 \\ 0 & \cos\phi & -\sin\phi \\ 0 & \sin\phi & \cos\phi \end{bmatrix}, \tag{2}$$

$$J_1(\eta_2) = \begin{bmatrix} \cos\psi\cos\theta & -\sin\psi\cos\phi + \cos\psi\sin\theta\sin\phi & \sin\psi\sin\phi + \cos\psi\sin\theta\cos\phi \\ \sin\psi\cos\theta & \cos\psi\cos\phi + \sin\psi\sin\theta\sin\phi & -\cos\psi\sin\phi + \sin\psi\sin\theta\cos\phi \\ -\sin\theta & \cos\theta\sin\phi & \cos\theta\cos\phi \end{bmatrix}$$

https://doi.org/10.1017/S0263574719000262 Published online by Cambridge University Press

Table II. Main dynamic constraints of the considered AUV.

Max/min of desired pitch angle	±20 deg
Rate of the pitch angle change	±2 deg/sec
Max/min of the desired yaw angle	±60 deg
Rate of the yaw angle change	±3 deg/sec
Elevator plane deflection	±20 deg
Rudder plane deflection	±20 deg

The relation between the orientation and angular velocities is explained through the $J_2(\eta_2)$:

$$\begin{bmatrix} \dot{\phi} \\ \dot{\theta} \\ \dot{\psi} \end{bmatrix} = J_2(\eta_2) \begin{bmatrix} p \\ q \\ r \end{bmatrix}, \quad J_2(\eta_2) = \begin{bmatrix} 1 & \sin\phi\tan\theta & \cos\phi\tan\theta \\ 0 & \cos\phi & -\sin\phi \\ 0 & \sin\phi/\cos\theta & \cos\phi/\cos\theta \end{bmatrix} \tag{3}$$

Note that when the pitch angle is ±90°, the $J_2(\eta_2)$ is singular. Euler–Rodrigues formula or quaternion rotations method has been applied for solving this problem, while the pitch angle of AUV is rarely greater or less than ±45° in practical terms. New states of AUV are calculated by Runge–Kutta's fourth order (RK4) approach or Euler method in each iteration.

2.3. Dynamic equations of motion

The six DOFs dynamics equation of AUV motion can be obtained based on the Newton–Euler formulation by[26] and presented in the general form as follows:

$$\begin{aligned} &\underbrace{M_{RB}\nu + C_{RB}(\nu)\nu}_{\text{rigid body terms}} + \underbrace{M_A\dot{\nu} + C_A(\nu)\nu + D(\nu)\nu}_{\text{hydrodynamic terms}} + \underbrace{g(\eta)}_{\text{hydrostatic terms}} \\ &= \underbrace{\tau_d}_{\text{external disturbances}} + \underbrace{\tau_u}_{\textit{forces and moments}} = \tau_d + Bu \end{aligned} \tag{4}$$

where $M_{RB} + M_A = M \in R^{6\times6}$ denotes the inertia matrix (including added mass), $C_{RB} + C_A = C : R^6 \to R^{6\times6}$ denotes the matrix of Coriolis and centripetal terms (including added mass), $D : R^6 \to R^{6\times6}$ indicates the hydrodynamic damping and lift matrix, $g : R^6 \to R^6$ is the vector of the gravitational forces and moments, $\tau_d \in R^6$ is the vector of the external disturbance, $\tau_u \in R^6$ is the vector of forces and moments acting on the AUV, $B \in R^{6\times2}$ is the distribution matrix, and $u = [\delta_R, \delta_E]^T \in R^2$ is the control input. δ_R, δ_E are used to define the control signals applied to the vertical and horizontal control surfaces (rudder and elevator), respectively. Performance of a nonlinear dynamic model is evaluated by open-loop tests in Fig. 2.

2.4. Design heading and diving controller through the Fuzzy proportional-derivative controllers

A formal methodology is provided by the Fuzzy controller to implement human heuristic knowledge on how to control the AUV with nonlinear complex dynamic, uncertainties, and disturbances. Here, three fuzzy proportional-derivative controllers (FPDCs) are designed for the AUV heading and diving control.[27] Each of them consists of two inputs, one output, and twenty-one rules. These rules are constructed based on the designer experience, AUV dynamic constraints (Table II), and knowledge from open-loop behavior.

In order to identify the open-loop behavior of AUV and tune the Fuzzy rules, three fundamental open-loop tests scenarios are designed: (1) direct course test, (2) zig-zag test, and (3) turning test. In the direct course test, angles of the rudder and elevator are fixed at zero and the surge speed of the AUV is stabilized. The maneuverability of the AUV in the horizontal plane is evaluated through the zig-zag test. In the zig-zag test, the elevator angle is fixed at zero and the rudder angle is toggled between ±20°. Turning radius of AUV is evaluated through the turning test. In this test, the rudder angle for $t > 75$ s is fixed at maximum deflection (+20°) and the elevator angle is fixed at zero. AUV behavior in the first, second, and third predefined open-loop tests is shown through the thick black solid line, dash red line, and thin blue line, in Fig. 2. In the first open-loop test AUV is stable in the horizontal plane; however, it has oscillation behavior in the vertical plane. In the second open-loop

https://doi.org/10.1017/S0263574719000262 Published online by Cambridge University Press

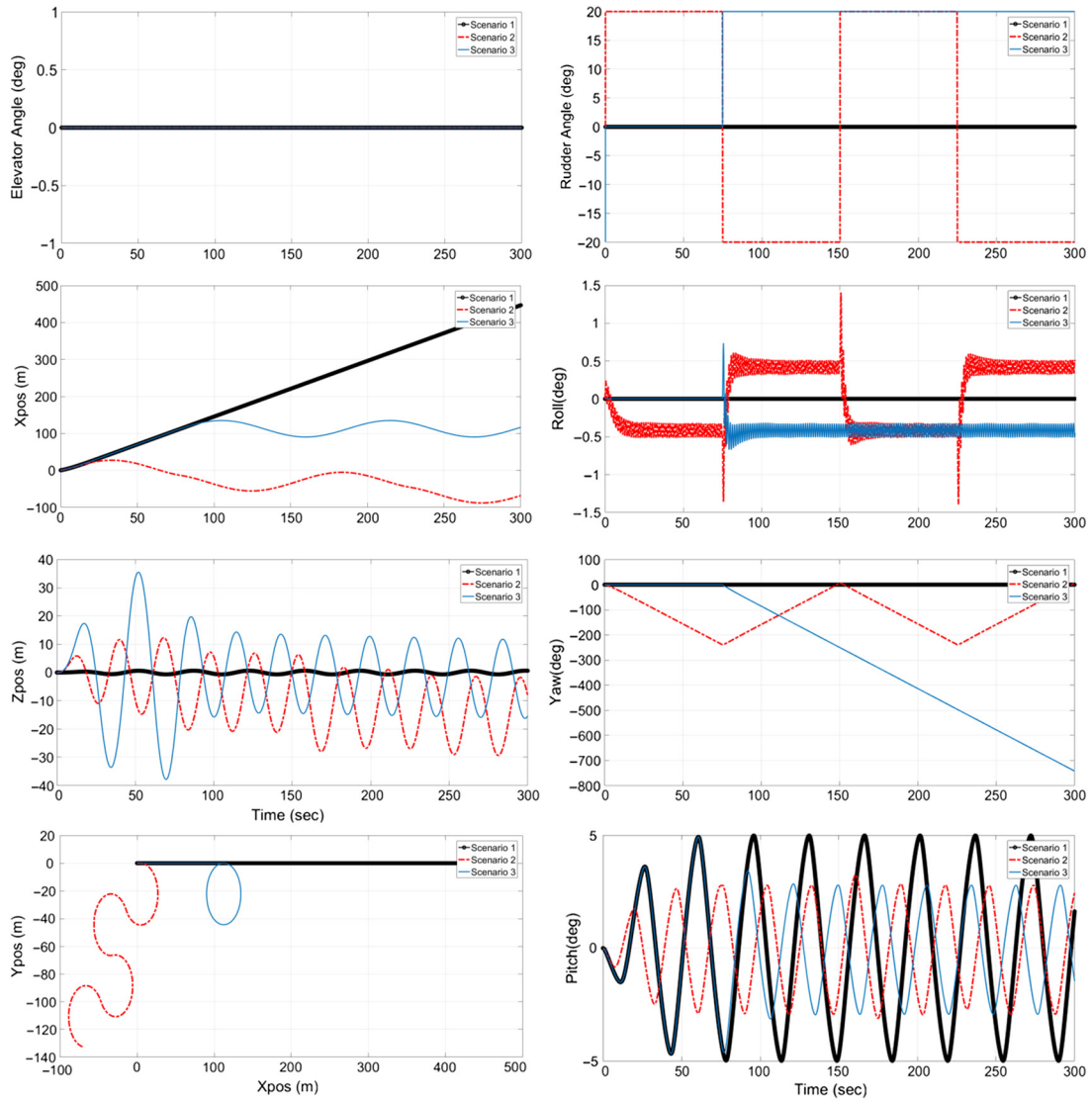

Fig. 2. AUV open-loop behavior in the first (direct course test), second (zig-zag test), and third (turning test) test scenarios.

test (zig-zag), AUV performs desired performance in the horizontal plane with small roll angles; however, its behavior in the vertical plane is similar to the first test and is oscillatory. In the third open-loop test (turning), AUV traverses a direct path up to $t < 75$ s and for $t > 75$ s starts to turn due to the rudder deflection. By considering the position and orientation of AUV, performance in the horizontal plane is acceptable. It is noteworthy that the AUV roll is neutralized by the vertical distance between the gravity center and buoyancy center.

By considering the results of three open-loop tests, an FPDC is proposed for the AUV heading control and two cascade structure FPDCs are designed for the AUV diving control (Fig. 3(a–b)). Depth error and its time-derivative (after fuzzified through the specific membership functions) are fed into the FPDC-1 as inputs in the outer loop to compute the desired pitch angle (DPA) through the fuzzy inference system (FIS) by 21 rules, as tabulated in Table III. Likewise, the pitch angle error and its time-derivative are fed into the FPDC-2 as inputs in the inner loop to compute the elevator plane deflection (EPD) through the FIS by 21 rules. The degree of fulfillment of each of the rules and their implications are calculated through the min-operator. The aggregation of the FPDC-1 is obtained through the max-operator. The crisp value of output is obtained through the centroid of area (CoA) method.

https://doi.org/10.1017/S0263574719000262 Published online by Cambridge University Press

Table III. Considered rules to compute the desired pitch angle in the diving controller (FPDC-1).

DPA		Depth error						
		BN	**N**	**SN**	**ZE**	**SP**	**P**	**BP**
Time-derivative of depth error	P	BP (1)	P (4)	SP (7)	SN (10)	SN (13)	N (16)	BN (19)
	Z	BP (2)	P (5)	SP (8)	ZE (11)	SN (14)	N (17)	BN (20)
	N	P (3)	SP (6)	ZE (9)	SP (12)	ZE (15)	SN (18)	N (21)

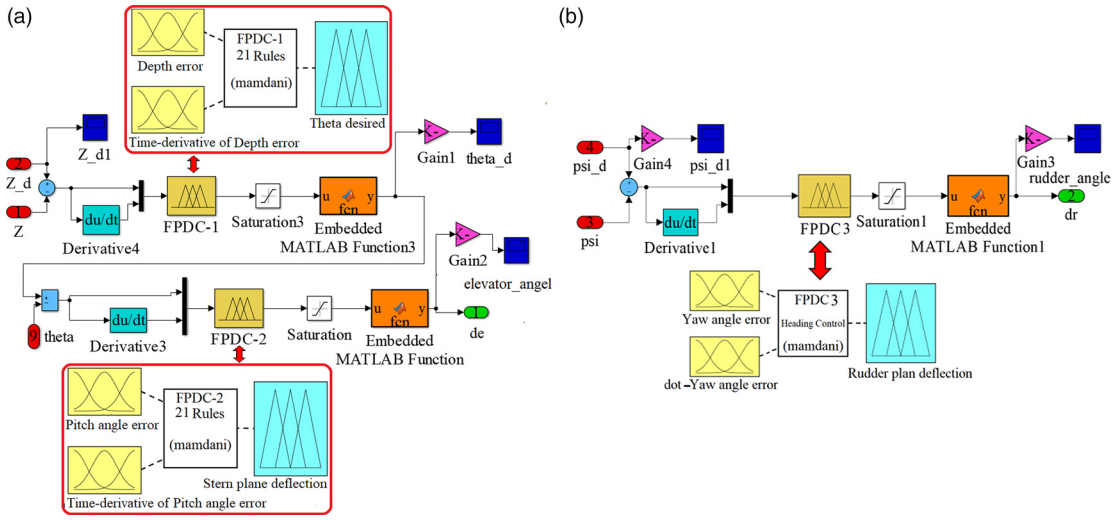

Fig. 3. AUV depth control through the two cascade structure FPDCs and AUV heading control through the FPDC.

The twenty-one fuzzy rules in FPDC-1 (Table III) are stated through the following structure:

Rule i: **If** $d_{E(AUV)}$ is $MF^i_{d_{E(AUV)}}$ and $rate_{d_{E(AUV)}}$ is $MF^i_{rate_{d_{E(AUV)}}}$ **Then** $DPA_{(AUV)}$ is $MF^i_{DPA_{(AUV)}}$, $i = 1, \ldots, 21$.

For example, rule No. 1 expresses that if the depth error of AUV ($d_{E(AUV)}$) after the fuzzification is big negative (BN) and if the time-derivative of depth error ($rate_{d_{E(AUV)}}$) after the fuzzification is positive (P) then in order to ensure that the AUV ideal performance, the DPA ($DPA_{(AUV)}$) is big positive (BP). In other words, the positive big DPA is needed in order to prevent the negative big depth error which is exacerbated by the positive time-derivative of depth error. As another example, consider the rule No. 9. In this rule, AUV depth error is small negative (SN) and it is neutralized through the negative time-derivative of depth error. Therefore, the required DPA is zero (ZE). In this way, other rules in the FPDCs are heuristically set as the same.

Heading controller consists of an FPDC with two inputs and one output (Fig. 3(b)). Inputs consist of yaw angle error and its time-derivative and the output is rudder plane deflection (RPD). This controller is designed through the same method that explains in the diving control.

Performance of FPDCs in AUV motion control is evaluated through the two different test cases with special maneuvers in Section 4 and is compared with the results of the proposed SMC through Table IV.

2.5. Design heading and diving controller through the conventional SMC

The tracking error vector in the horizontal plane is defined as follows:

$$\tilde{x} = x - x_d = \begin{bmatrix} v \\ r \\ \psi \end{bmatrix} - \begin{bmatrix} v_d \\ r_d \\ \psi_d \end{bmatrix} \tag{5}$$

https://doi.org/10.1017/S0263574719000262 Published online by Cambridge University Press

Table IV. Comparison of the results the three existing conventional approaches with the proposed SMC in the AUV motion control through the two test cases.

	PID		**Conventional SMC**		**Proposed SMC**		**FPDC**	
	First test case	**Second test case**	**First test case**	**Second test case**	**First test case**	**Second test case**	**First test case**	**Second test case**
Chattering phenomenon	Eliminated	Eliminated	High	High	Ignorable	Ignorable	Eliminated	Eliminated
Rudder control signal amplitude	High	High	High	Middle	High	Small	High	Middle
Elevator control signal amplitude	High	High	Middle	Middle	Small	Small	High	High
Tracking the desired trajectory	With oscillation	With oscillation	Same	Same	Same	Same	With a slow rise time	With a slow rise time
Overshoot	About 10%	About 10%	Ignorable	Ignorable	Eliminated	Eliminated	Eliminated	Eliminated

The desired states in this equation are defined using the sub-index (d). Sum of the weighted components of the tracking error vector in the horizontal plane is applied to define the sliding surface:

$$\sigma = s^T \tilde{x} = \begin{bmatrix} s_1 & s_2 & s_3 \end{bmatrix} \begin{bmatrix} x_1 - x_{1d} \\ x_2 - x_{2d} \\ x_3 - x_{3d} \end{bmatrix} = s_1(v - v_d) + s_2(r - r_d) + s_3(\psi - \psi_d) = 0 \tag{6}$$

The sliding surface is simplified provided that the desired value for $v_d = r_d = 0$:

$$\sigma = s_1\,(v) + s_2\,(r) + s_3\,(\psi - \psi_d) \tag{7}$$

By considering the content that is published on[17] the control signal applied to the vertical actuator (rudder) is designed as follows:

$$\delta_R = \frac{\left[-\eta_{S-G} sat\left(\sigma / \phi_{B-L-T}\right) - (s_1 a_{11} + s_2 a_{21})\, v\right] - (s_1 a_{12} + s_2 a_{22} + s_3)\, r}{s_1 b_1 + s_2 b_2} \tag{8}$$

where ϕ_{B-L-T} is the boundary layer thickness around the sliding surface, η_{S-G} is the switching gain, and $[s_1, s_2, s_3]$ are the sliding surface coefficients. By considering the AUV parametric model in the horizontal plane, Matrix A is $A = [a_{ij}]$ $i\&j = 1, \ldots, 3$ and Matrix B is $B = [b_{ij}]$ $i = 1, \ldots, 3$ & $j = 1$ which components are described below and their values are tabulated in the Appendix:

$$\begin{gathered} a_{11} = \frac{Y_v}{m - Y_{\dot{v}}},\ a_{12} = \frac{Y_r - mU}{m - Y_{\dot{v}}},\ a_{13} = 0,\ a_{21} = \frac{N_v}{I_{zz} - N_{\dot{r}}},\ a_{22} = \frac{N_r - mUx_g}{I_{zz} - N_{\dot{r}}}, \\ a_{23} = 0,\ a_{31} = 0,\ a_{32} = 1,\ a_{33} = 0,\ b_{11} = \frac{Y_{\delta_r}}{m - Y_{\dot{v}}},\ b_{21} = \frac{N_{\delta_r}}{I_{zz} - N_{\dot{r}}},\ b_{31} = 0 \end{gathered} \tag{9}$$

In order to assure the state-space variables asymptotically converge to their desired value $\left(\lim_{t\to\infty}(x - x_d) \to 0\right)$, the sliding surface is designed by considering the following conditions:

$$\begin{gathered} \lim_{t\to\infty} \sigma \to 0, \\ \lim_{t\to\infty} \dot{\sigma} \to 0 \end{gathered} \tag{10}$$

The system state variables are guaranteed to converge to the sliding surface and maintain at there, and also system is stabilized on the manifold in a finite time, if the Lyapunov candidate function $\left(V(\sigma) = \frac{1}{2}\sigma^2\right)$ satisfies the following condition:

$$\dot{V}(\sigma) = \frac{1}{2}\frac{d}{dt}\sigma^2 = \sigma\dot{\sigma} \leq -\eta_{S-G}\,|\sigma| \tag{11}$$

https://doi.org/10.1017/S0263574719000262 Published online by Cambridge University Press

By expanding the above equation:

$$\begin{aligned}&\dot{\sigma} = S^T(\dot{x} - \dot{x}_d) \le -\eta_{S-G} sgn(\sigma)\\ &\Rightarrow \dot{\sigma} = S^T(Ax + Bu - \dot{x}_d) \le -\eta_{S-G} sgn(\sigma)\\ &u = -(S^TB)^{-1}S^TAx - (S^TB)^{-1}S^T\dot{x}_d - (S^TB)^{-1}\eta_{S-G} sgn(\sigma)\end{aligned} \tag{12}$$

By considering matrix A and B that their components are described in Eq. (9), the time-derivative of the sliding surface in the horizontal plane is defined as follows:

$$\begin{aligned}\dot{\sigma} = s_1(\dot{v}) + s_2(\dot{r}) + s_3\left(\dot{\psi}\right) &= s_1(a_{11}v + a_{12}r + b_1\delta_R) + s_2(a_{21}v + a_{22}r + b_2\delta_R) + s_3(r)\\ &\le -\eta_{S-G} sat\left({}^{\sigma}/_{\phi_{B-L-T}}\right)\end{aligned} \tag{13}$$

Desired states are constant here; therefore, its time-derivative ($\dot{x}_d$) is zero. To prevent the chattering phenomenon in the control signal, the signum function is replaced by the saturation function which is defined in Eq. (14) and a thin boundary layer (ϕ_{B-L-T}) is designed in the neighborhood of the sliding surface:

$$sat\left({}^{\sigma}/_{\phi_{B-L-T}}\right) = \begin{cases} {}^{\sigma}/_{\phi_{B-L-T}} & if \left|{}^{\sigma}/_{\phi_{B-L-T}}\right| \le 1\\ \text{sgn}\left({}^{\sigma}/_{\phi_{B-L-T}}\right) & \text{otherwise}\end{cases} \tag{14}$$

Consequently, the control signal applied to the vertical actuators (rudders) consists of two linear and nonlinear parts:

$$\begin{aligned}&u = \hat{u} + \bar{u} \quad \Leftrightarrow \quad \delta_R = \hat{\delta}_R + \bar{\delta}_R,\\ &u_{linear} = \hat{u} = \hat{\delta}_R,\\ &u_{nonlinear} = \bar{u} = \bar{\delta}_R\end{aligned} \tag{15}$$

The linear part of the control signal is, in fact, a feedback of the system state that is responsible for ensuring the desired system performance when the state lays on the sliding surface:

$$\hat{\delta}_R = \frac{-\left[(s_3 + s_1a_{12} + s_2a_{22})\, r + (s_1a_{11} + s_2a_{21})\, v\right]}{s_1b_1 + s_2b_2} = -\left(S^TB\right)^{-1}S^TAx = -Kx \tag{16}$$

where (k) is the feedback gain vector which is calculated by the pole placement method or by minimizing an optimality index through the linear quadratic regulator (LQR) defined as follows:

$$J = \int_0^{\infty}\left(x^TQx + \delta^TR\delta\right)dt \tag{17}$$

where x is the state vector, δ is the control input, Q is the semi-positive constant symmetric weighted matrix, and R is the positive constant symmetric weighted matrix. The feedback gain (K) for minimizing the optimality index in Eq. (17) for initial conditions is yield through:

$$K = R^{-1}B^TP \rightarrow K = LQR(A, B, Q, R) \tag{18}$$

where matrix P is obtained by solving the algebraic Riccati equations (ARE):

$$PA + A^TP - PB^{-1}RBP + Q = 0 \tag{19}$$

By applying matrix P, the feedback gain (K) is yield. The coefficients of the sliding surface $[s_1, s_2, s_3]$ are calculated according to the feedback gain specified by the LQR. For this purpose, the closed-loop state matrix is expressed as follows:

$$\begin{aligned}&\dot{\sigma} = S^T\dot{X} = S^TA_{cl}X = 0\,,\\ &S^TA_{cl} = [0] \quad or \quad A_{cl}^TS = [0]\end{aligned} \tag{20}$$

https://doi.org/10.1017/S0263574719000262 Published online by Cambridge University Press

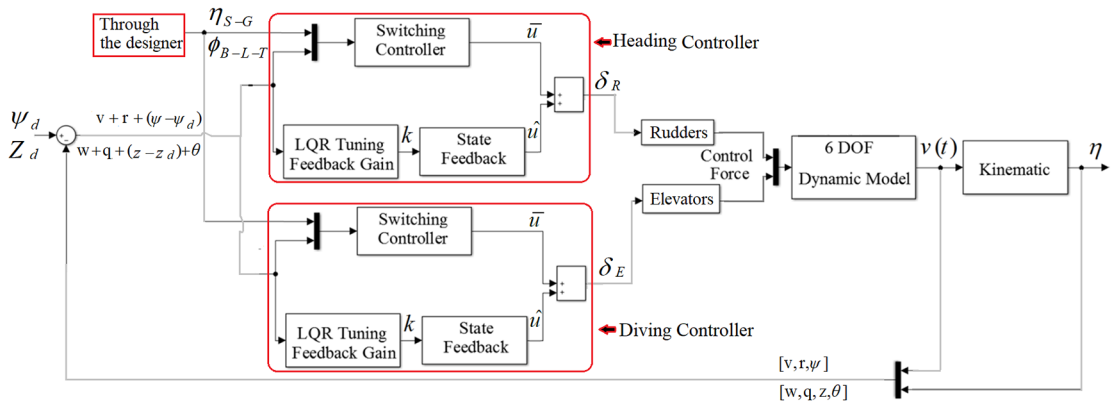

Fig. 4. AUV motion control by the conventional SMC.

The coefficients of the sliding surface are obtained by the left eigenvector corresponding to the null eigenvalue of the closed-loop state matrix:

$$S^T = \begin{bmatrix} s_1 & s_2 & s_3 \end{bmatrix} = Eigenvector \ \left(A_{cl}^T\right)_{Eigenvalue=Null} \tag{21}$$

The nonlinear part of the controller in the SMC is responsible to the compensation of any unstructured dynamic behavior that causes the system state to exit from the sliding surface and maintains the system states on the sliding surface:

$$\bar{\delta}_R = \frac{-\eta_{S-G} sat\left(\sigma/\phi_{B-L-T}\right)}{s_1 b_1 + s_2 b_2} = -\left(S^T B\right)^{-1} \eta_{S-G} sat\left(\sigma/\phi_{B-L-T}\right) \tag{22}$$

The closed-loop system equation when the system state is located on the sliding surface is presented by

$$\begin{aligned} \dot{x} &= Ax + B\hat{\delta}_R, \\ \dot{x} &= [A - BK]\, x, \\ \dot{x} &= [A_{cl}]\, x \end{aligned} \tag{23}$$

where $[A_{cl}]$ is the closed-loop state matrix.

The tracking error vector in the vertical plane is defined as follows:

$$\tilde{x} = x - x_d = \begin{bmatrix} w \\ q \\ z \\ \theta \end{bmatrix} - \begin{bmatrix} w_d \\ q_d \\ z_d \\ \theta_d \end{bmatrix} \tag{24}$$

The sliding surface in the vertical plane is defined by using weighted components of tracking error vector as follows:

$$\sigma = \mathbf{S}^T \tilde{\mathbf{X}} = \begin{bmatrix} s_1 & s_2 & s_3 & s_4 \end{bmatrix} \begin{bmatrix} x_1 - x_{1d} \\ x_2 - x_{2d} \\ x_3 - x_{3d} \\ x_4 - x_{4d} \end{bmatrix} = s_1 (w - w_d) + s_2 (q - q_d) + s_3 (z - z_d) + s_4 (\theta - \theta_d) = 0 \tag{25}$$

The control input in the vertical plane consists of linear and nonlinear parts and these parts are designed by the same method that explains in the heading control. The conventional SMC in Fig. 4 is applied to the nonlinear dynamic model of AUV in Eq. (4), and the results are compared with the proposed method and two existing approaches in the AUV motion control through the two test cases with special maneuvers in 3D space in the following section.

https://doi.org/10.1017/S0263574719000262 Published online by Cambridge University Press

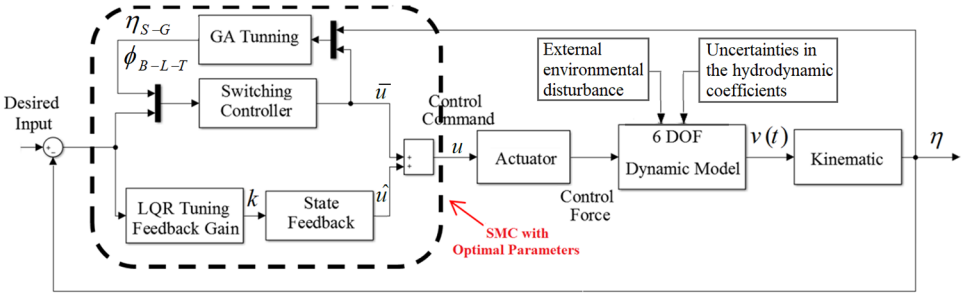

Fig. 5. Block diagram of the proposed SMC.

3. Proposed SMC

Sliding surface coefficients (s_1, s_2, s_3) and the feedback gain (k) in the linear part of the SMC law are designed by the pole placement or LQR method, while the boundary layer thickness (ϕ_{B-L-T}) and switching gain (η_{S-G}) in the nonlinear part of SMC law are usually designed by trial-and-error method. Chattering phenomenon, the amplitude of control signal, steady-state error, reaching time, settling time, maximum overshoot, and other performance features of the system are affected by the controller parameter selection.

Here, a heuristic approach is used for eliminating the human experience needs in parameters' selection which is evaluated through the PIL test. PIL is a real-time and cost-effective test usually run before the FAT, HAT, and SAT tests and after the software-in-the-loop (SIL) test at the detailed design stage. In this context, the execution codes are debugged without actual AUV involvement which leads to a reduction in field tests costs. The block diagram of the proposed SMC is illustrated in Fig. 5.

3.1. Designing the boundary layer thickness and switching gain through the GA

To prevent the chattering phenomenon in control signals, a thin boundary layer is designed in the neighborhood of the sliding surface. Although the chattering phenomenon in control signals and noise measurement effect are reduced by the boundary layer thickness (ϕ_{B-L-T}), the tracking performance, and robustness of the system could be compromised. In this context, optimal designing of the boundary layer thickness becomes more essential. Several methods such as hand-tuning, adaptive tuning, fuzzy tuning, and time-varying tuning with different strategies are proposed in the available studies.[28,29]

Another parameter in the nonlinear part of SMC law is the switching gain (η_{S-G}) which is designed to compensate the unmodeled dynamics, model uncertainty, and external disturbance. Designing a great switching gain could exacerbate the amplitude of chattering and on the contrary, it could undermine the convergence of the system. For this purpose, knowing the bounds on system uncertainties and disturbance amplitude is a must for optimal selection of switching gain. Several methods such as trial and error, adaptive tuning, soft tuning, and time-varying tuning are proposed in the available studies,[30] regarding switching gain design.

The boundary layer thickness and switching gain are designed through GA. For this purpose, 50 chromosomes are used in forming the early population for optimizing the fitness function (line 3 in Algorithm 1). Each chromosome has 16 genes, Fig. 6. One-half of these genes are applied in describing the switching gain and the other half is applied in describing the boundary layer thickness (line 4 in Algorithm 1). The probability of mutation and crossover are considered as $p_{mutation} = 0.01$ and $p_{crossover} = 0.75$, respectively. The roulette wheel is applied to select the chromosome (lines 5–6, 9 in Algorithm 1). The fitness function for the heading and diving controllers are designed, respectively, as follows:

$$\begin{aligned} &J_{horizontal} = \int_0^T e_\psi^2(\tau)d\tau + \int_0^T \delta_R^2\ (\tau)\ d\tau, \\ &e_\psi = \psi_d - \psi \\ &J_{vertical} = \int_0^T e_z^2(\tau)d\tau + \int_0^T e_\theta^2(\tau)d\tau + \int_0^T \delta_E^2(\tau)d\tau, \\ &e_z = Z_d - Z, \qquad e_\theta = \theta_d - \theta \end{aligned} \tag{26}$$

https://doi.org/10.1017/S0263574719000262 Published online by Cambridge University Press

Algorithm 1 Proposed SMC

Begin

1: Desired trajectory ← $[\psi_d, Z_d]$ ▷ *by Section.* 4
2: U_P ← Maximum iteration for optimizing the switching gain and boundary layer thickness
3: N ← Population size
4: $n = \left[\eta_{S-G_i}, \phi_{B-L-T_i}\right]$ ← Initial random population (N)
5: P_M ← Mutation rate
6: P_C ← Crossover rate
7: $[n]$ ← Rank initial random population (n, J)
8: **While** $i \leq U_P$ **or** terminate condition is NOT **do**
9: $S_P = \left[\eta_{S-G}, \phi_{B-L-T}\right]$ ← Roulette wheel (n)
10: Crossover(S_P)
11: Mutation(S_P)
12: $[\delta_R, \delta_E]$ ← SMC (desired trajectory, S_P) ▷ *by Eq.* 15
13: $[\psi, Z, \theta]$ ← Six degree-of-freedom nonlinear AUV model (δ_R, δ_E) ▷ *by Eq.* 4
14: $[J(S_P)_{horizontal}, J(S_P)_{vertical}]$ ← Fitness function (*Desired trajectory*, ψ, Z, θ) ▷ *by Eq.* 26
15: $n \leftarrow S_P \cup n$
16: n ← Rank new population (n)
17: n ← Selected best population (n, J)
18: **End While**
19: Elite solution ← Get best (n, J)
20: $[\delta_R, \delta_E]$ ← SMC implemented on an SBC through the xPC Target and evaluated by the PIL test (Desired trajectory, Elite solution) ▷ *by Section.* 3.3
21: Behavior of AUV in 3D space ← Six degree-of-freedom nonlinear AUV model (δ_R, δ_E)

End

$$J_{horizontal} = \int_0^T e_\psi^2 \ \tau \ d\tau + \int_0^T \delta_R^2 \ \tau \ d\tau,$$

$$e_\psi = \psi_d - \psi$$

$$J_{vertical} = \int_0^T e_z^2 \ \tau \ d\tau + \int_0^T e_\theta^2 \ \tau \ d\tau + \int_0^T \delta_E^2 \ \tau \ d\tau,$$

$$e_z = Z_d - Z \quad , \quad e_\theta = \theta_d - \theta$$

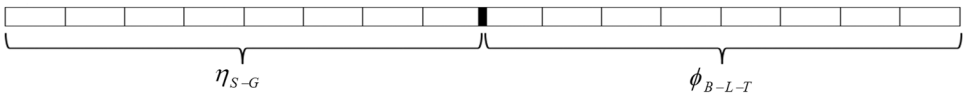

Fig. 6. A chromosome with information about the switching gain and boundary layer thickness.

The selected chromosome and the desired trajectory in the considered test case are used by the SMC and the control signals are computed to be applied in horizontal and vertical actuators (line 12 in Algorithm 1). The fitness function is calculated for each chromosome (new boundary layer thickness and switching gain) by considering the AUV motion control behavior in 3D space (line 14 in Algorithm 1). The newly generated population is ranked and converged into the optimal value in the *i*th iteration (lines 15–17 in Algorithm 1). The elite solution is implemented on an SBC through the xPC Target and evaluated by the PIL test (lines 19–21 in Algorithm 1). The pseudo-code of the proposed SMC is expressed in Algorithm 1. The switching gains and boundary layer thickness in vertical and horizontal planes are converged into the optimal point through GA, Fig. 7.

3.2. Robustness of the proposed SMC in the presence of external disturbance and model uncertainties

In order to demonstrate the robustness of the proposed SMC in the presence of external disturbances and model uncertainties as shown in Fig. 5, the following two scenarios are considered.

https://doi.org/10.1017/S0263574719000262 Published online by Cambridge University Press

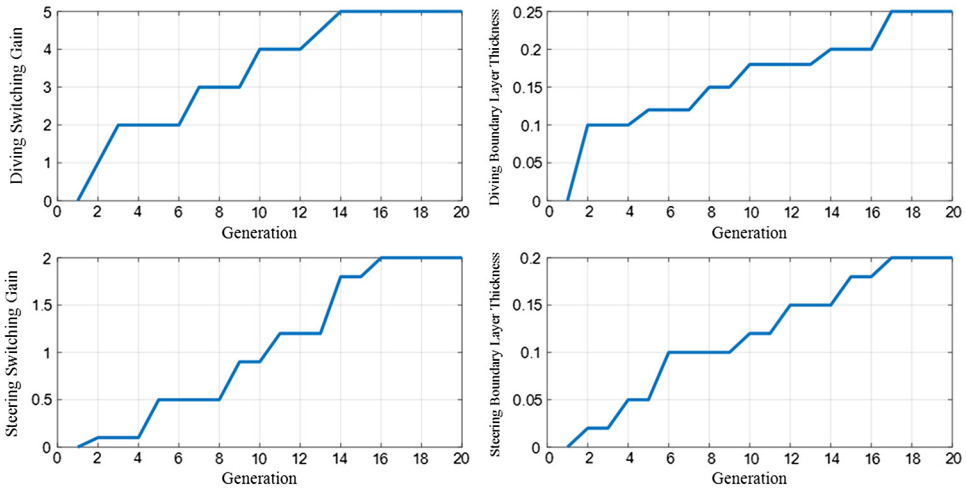

Fig. 7. Switching gain and boundary layer thickness are converged into the optimal point in the heading and diving controller in the proposed SMC.

Scenario 1: Assuming that moments of inertia and the AUV characteristic (mass) are increased by 15% with respect to their nominal values and external disturbances are generated based on the following equation:

$$\begin{aligned} &M\dot{v} + C(v)v + D(v)v + G(\eta) = \tau_d + \tau_u \\ &d_{surge} = \begin{cases} 5 + 3^*\sin(0.1^*t) - 7^*\cos(0.1^*t) & 60 < t < 70 \\ 3 - 5^*\sin(0.1^*t) - 7^*\cos(0.1^*t) & 130 < t < 150 \end{cases} \\ &d_{sway} = \begin{cases} 4 - 3^*\sin(0.1^*t) - 5^*\cos(0.1^*t) & 60 < t < 70 \\ -4 + 3^*\sin(0.1^*t) + 5^*\cos(0.1^*t) & 130 < t < 150 \end{cases} \end{aligned} \tag{27}$$

Scenario 2: Assuming that moments of inertia and the AUV characteristic (mass) are increased by 35% with respect to their nominal values and external disturbances are generated based on the following equation:

$$\begin{aligned} &M\dot{v} + C(v)v + D(v)v + G(\eta) = \tau_d + \tau_u \\ &d_{surge} = \begin{cases} -5 + 7^*\text{randn}(1,\,1) + 3^*\sin(0.1^*t) - 2^*\cos(0.1^*t) & 50 < t < 60 \\ 5 - 8^*\text{randn}(1,\,1) + 4^*\sin(0.1^*t) - 4^*\cos(0.1^*t) & 115 < t < 135 \end{cases} \\ &d_{sway} = \begin{cases} 8 + 8^*\text{randn}(1,\,1) - 3^*\sin(0.1^*t) - 3^*\cos(0.1^*t) & 50 < t < 60 \\ 4 - 8^*\text{randn}(1,\,1) + 4^*\sin(0.1^*t) + 5^*\cos(0.1^*t) & 115 < t < 135 \end{cases} \end{aligned} \tag{28}$$

where $\tau_u \in R^6$ is the vector of forces and moments acting on the robot and $\tau_d \in R^6$ is the external environmental disturbance. In Eqs. 27 and 28, waves, currents, and random environmental disturbances are simulated through the sinusoidal functions, constant terms, and Randn function,[31] respectively.

In these scenarios, the AUV has a step maneuver of $+45°$ amplitude in the horizontal plane up to $t < 100$ s while within $100 < t < 170$ s the AUV has a step maneuver with $-45°$ amplitude. For $170 < t < 270$ s the desired yaw angle for the AUV is $+25°$ while within $270 < t < 350$ s the AUV has a step maneuver with $-25°$ amplitude and for $t > 350$ s the desired yaw angle for the AUV is $0°$. The AUV depth is changed by the ramp function in the vertical plane and the surge speed of the AUV is stabilized.

Desired trajectory in Scenario 1 by considering %15 uncertainties and external environmental disturbances is tracked through the AUV without steady-state error (Fig. 8). In Scenario 2 by increasing uncertainty and amplitude of disturbance, a small steady-state error is observed (Fig. 8). The amplitude of control signals applied to the actuators through the proposed SMC is increased in Scenario 2 but is acceptable, and also a transient error in the AUV yaw angle is observed. However, the desired trajectory is tracked through the proposed SMC without oscillation and overshoot, and the AUV performance is appropriate.

https://doi.org/10.1017/S0263574719000262 Published online by Cambridge University Press

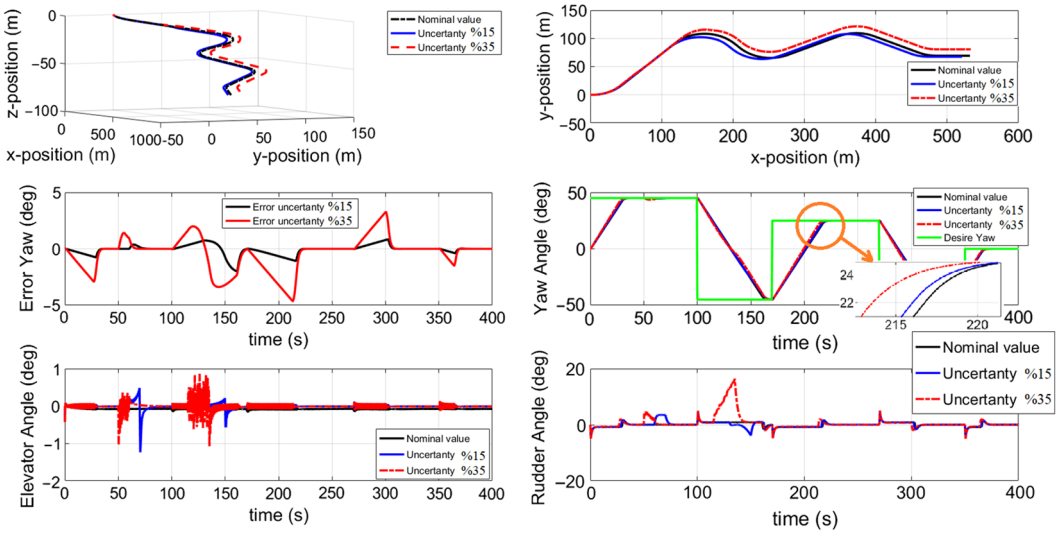

Fig. 8. Desired and actual behavior of AUV in Scenarios 1 and 2.

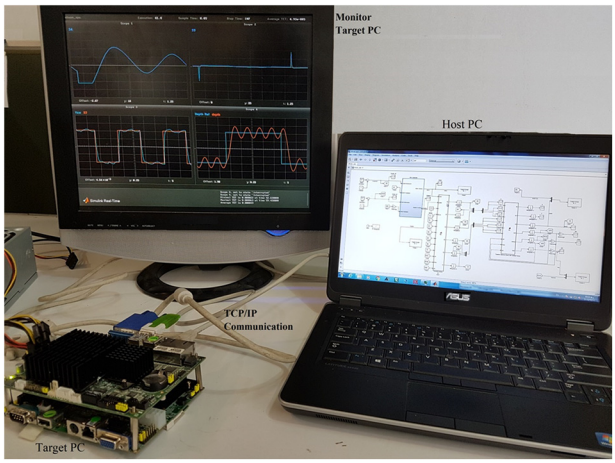

Fig. 9. PIL test setup.

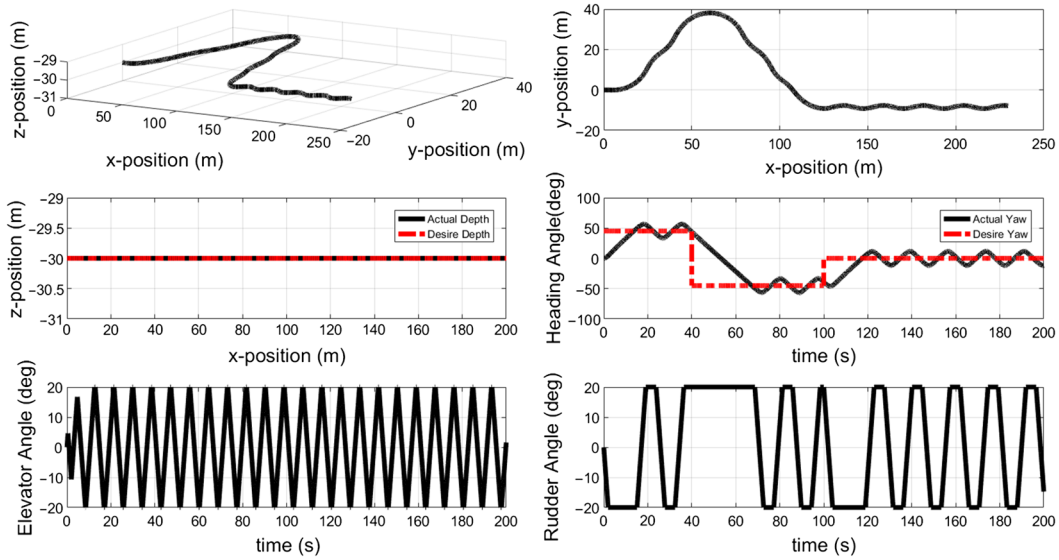

Fig. 10. The AUV motion control through the PID in the first test case.

https://doi.org/10.1017/S0263574719000262 Published online by Cambridge University Press

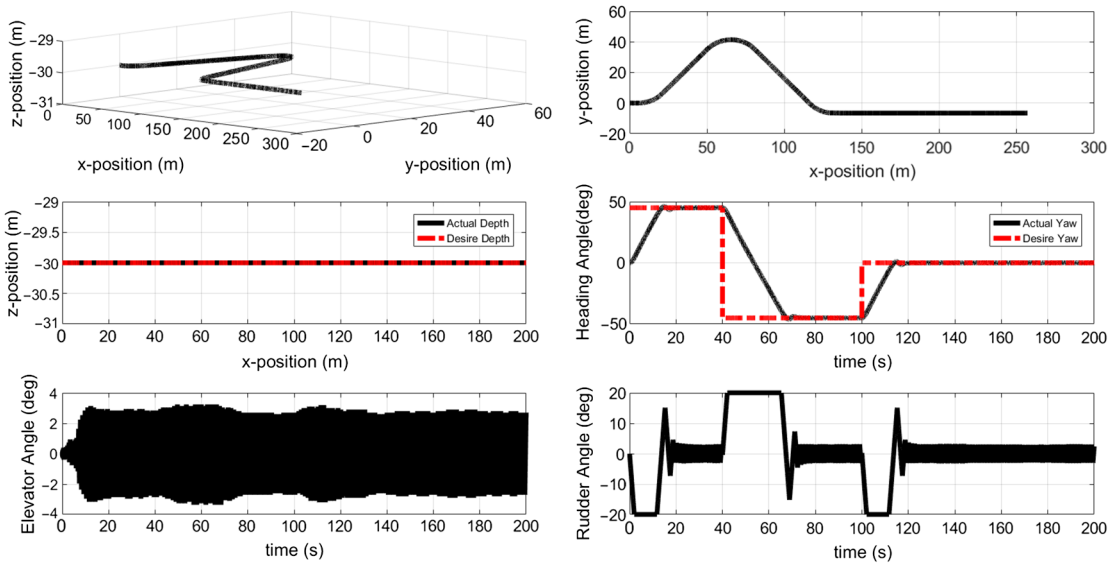

Fig. 11. The AUV motion control through the conventional SMC in the first test case.

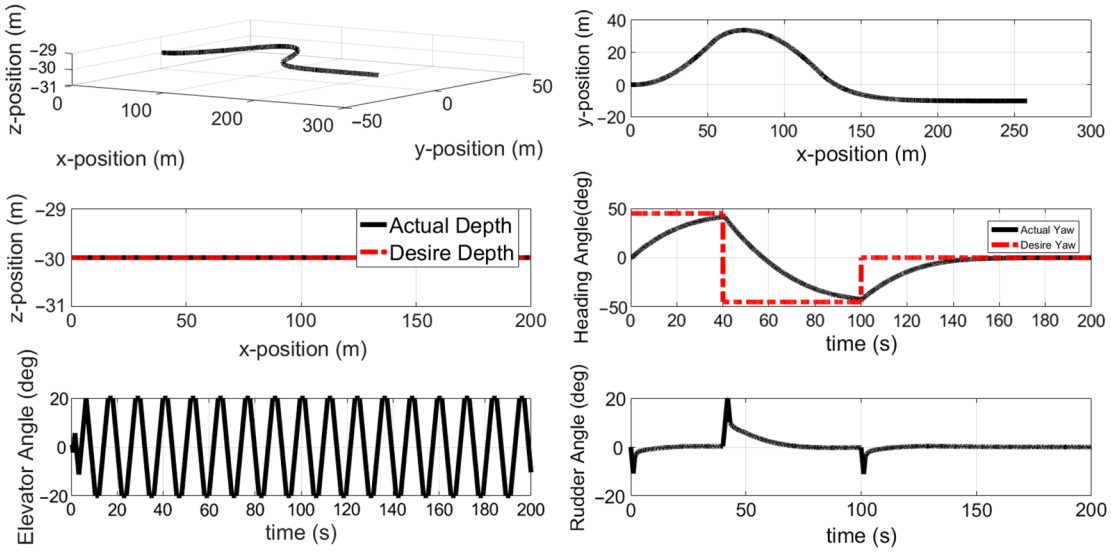

Fig. 12. The AUV motion control through the FPDCs in the first test case.

3.3. Implementation of the proposed SMC

The abilities of the proposed SMC with a heuristic approach in designing the nonlinear parameters are evaluated through the PIL tests in a cost-effective manner before the actual AUV becomes involved in the field tests. PIL test is an intermediate test for evaluating a motion control algorithm which usually runs before the FAT, HAT, and SAT and after the SIL. By this way, the execution codes are verified in the higher level than SIL test and many of the probabilistic difficulties are identified before the field tests. Therefore, the costs of field tests and its risks are reduced.

For this purpose, execution codes are generated through the xPC Target builder and implemented on a separate SBC by applying TCP/IP communication protocol through a maximum 10 Mbit/sec data transfer rate. The setup of the PIL test is shown in Fig. 9 and consists of three major parts of: host PC, target PC, and xPC Target. The host PC is a laptop with an Intel Core i7-4700HQ @ 2.4GHz and 8GB RAM, the target PC is an Axiomtek SBC 84710 and xPC Target is a real-time and cost-effective procedure for running the PIL test. The model of the proposed SMC is built in the host PC and its kernel code is transferred to the target PC for execution.

https://doi.org/10.1017/S0263574719000262 Published online by Cambridge University Press

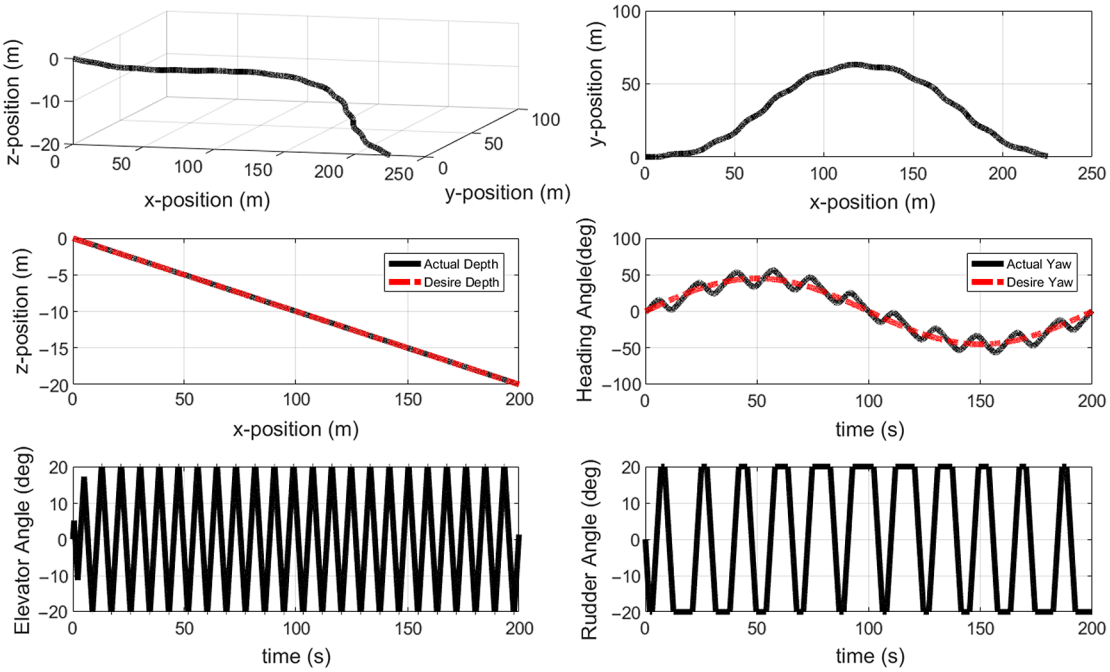

Fig. 13. The AUV motion control through the PID in the second test case.

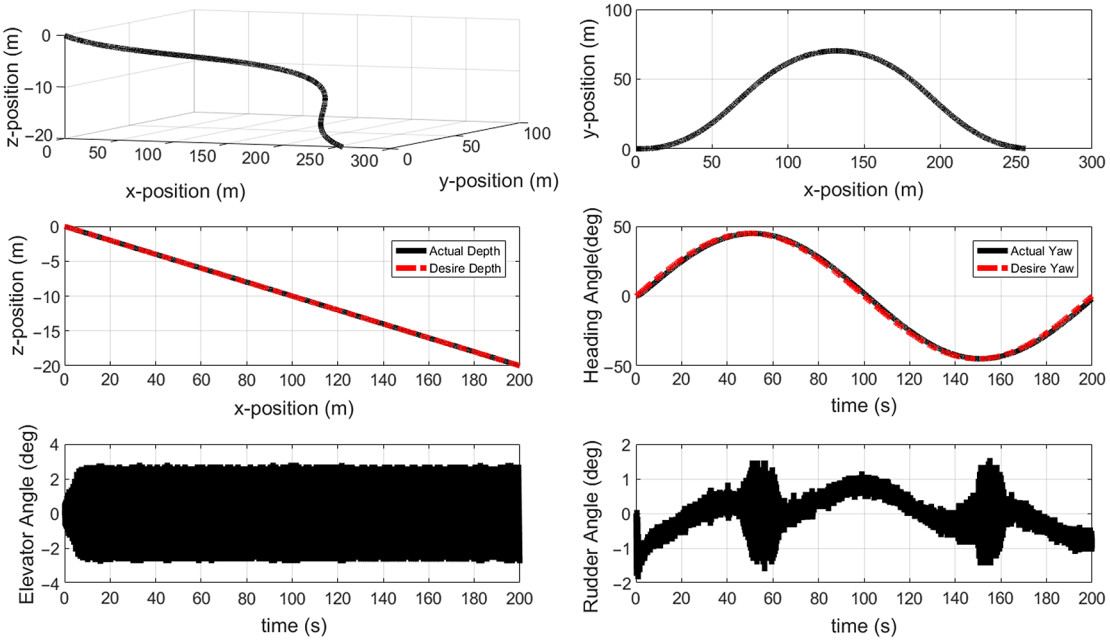

Fig. 14. The AUV motion control through the conventional SMC in the second test case.

4. Test Cases

To evaluate the motion control ability of the proposed SMC in the AUV motion control, two test cases with special maneuvers are designed in a 3D space.

In the first test case, the AUV has a step maneuver of 45° amplitude in the horizontal plane up to $t < 40$ while within $40 < t < 100$ the AUV has a step maneuver with $-45°$ amplitude and for $t > 100$ the desired yaw angle for the AUV is 0°. The AUV depth is fixed at 30 m in the vertical plane and surge speed along the longitudinal axis is stabilized.

https://doi.org/10.1017/S0263574719000262 Published online by Cambridge University Press

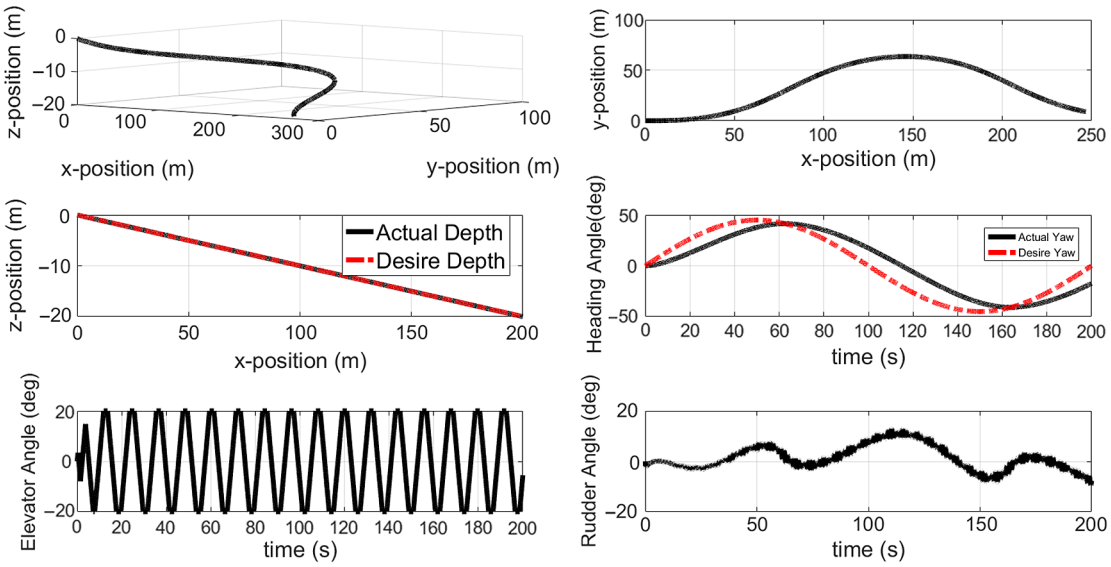

Fig. 15. The AUV motion control through the FPDCs in the second test case.

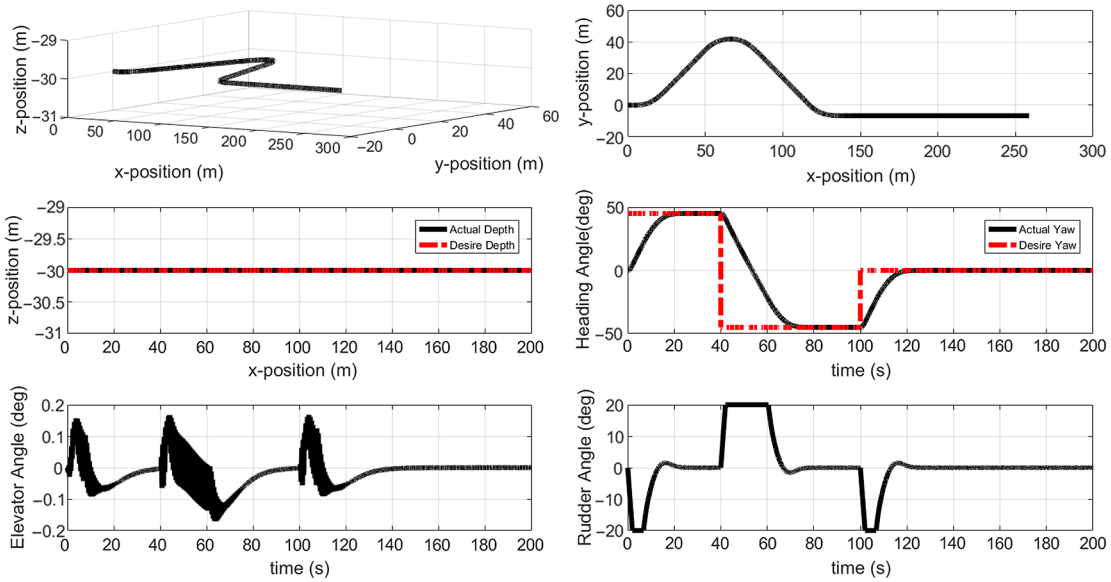

Fig. 16. The AUV motion control through the proposed SMC in the first test case.

In the second test case, the AUV has a sinusoidal maneuver with 45° amplitude in the horizontal plane, the AUV depth is changed by the ramp function in the vertical plane and the surge speed of the AUV is stabilized.

The results of the first test case are illustrated in Figs. 10–12 and 16 which include: AUV motion in the 3D space and horizontal plane, tracking the desired depth and heading angle, control signal applied to the rudder and elevator through the PID, conventional SMC, FPDC, and proposed SMC. Likewise, the results of the second test case are illustrated in Figs. 13–15 and 17.

The desired trajectory through the PID control is tracked by the AUV with oscillation and overshoot. The amplitude of control signals applied to the actuators through the PID are high in the first and second test case; however, the chattering is not observed in Figs. 10 and 13.

Oscillation and overshoot in tracking the desired trajectory are reduced through the conventional SMC in the first and second test case while the chattering phenomenon is observed in the control signal (Figs. 11 and 14).

https://doi.org/10.1017/S0263574719000262 Published online by Cambridge University Press

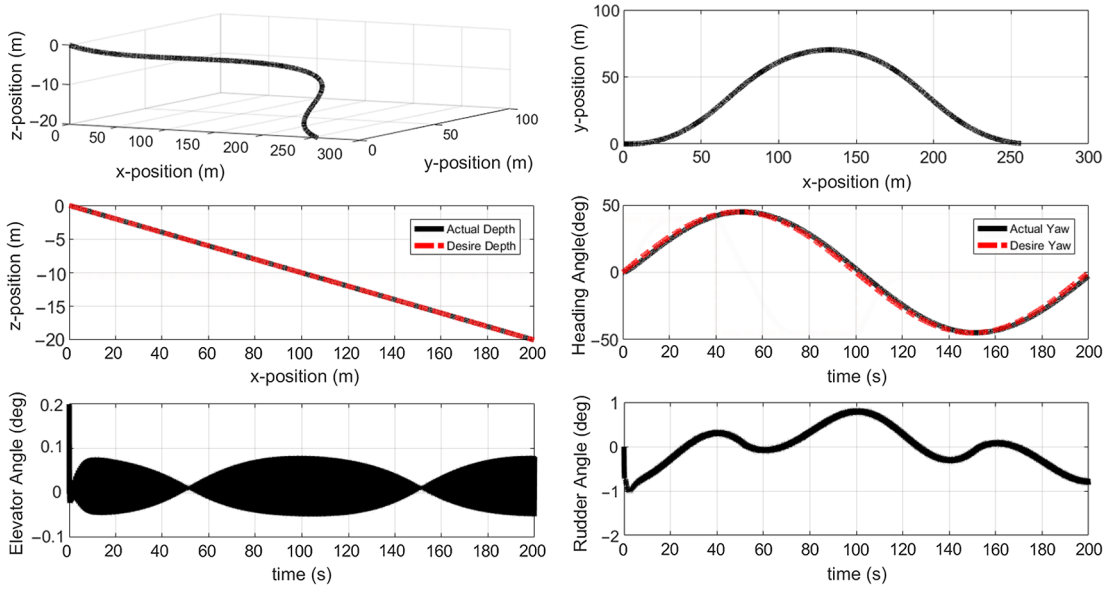

Fig. 17. The AUV motion control through the proposed SMC in the second test case.

The desired trajectory is tracked by the AUV through the FPDCs with a slow rise time. The amplitude of control signals applied to the actuators through the FPDCs are high in the first and second test case; however, the chattering, oscillation, and overshoot are not observed in Figs. 12 and 15.

AUV behaviors in tracking the desired trajectory through the proposed approach are satisfactory in both test cases. The amplitude of control signals are reduced and chattering phenomenon is eliminated in the control signals Figs. 16 and 17. The findings of the PIL test in both test cases through the PID, FPDCs, conventional, and proposed SMC are tabulated in Table IV.

5. Conclusion

The SMC with optimal parameters in the nonlinear part of control law which includes the boundary layer thickness and switching gain is proposed and evaluated through the PIL test. For this purpose, two different fitness functions are presented in the horizontal and vertical planes and a heuristic method is applied for their optimization. The proposed method is implemented on an Axiomtek SBC 84710 for two test cases with different scenarios through the xPC Target, followed by evaluating its abilities in AUV motion control through the PIL test in the presence of external disturbances and model uncertainties. This SBC is used as the high-level processor in the actual AUV. Therefore, the designed approach is applicable and is more reliable than SIL test. Here, before the actual AUV becomes involved in FAT, HAT, and SAT the execution codes are debugged and verified in a cost-effective manner, which in turn reduce the risks thereof. In the proposed approach human experience, knowledge on the amplitude of disturbances and information about the bounds of system uncertainties are not necessary. Hence, trial-and-error efforts by the designer(s) are reduced. The results obtained through the PIL tests in both test cases indicate that the chattering phenomenon and amplitude of control signal applied to the actuators are reduced. Furthermore, the performance of the AUV motion control system from a variety of perspectives such as maximum overshoot and tracking desired trajectory is improved in comparison with the existing three conventional AUV motion control approaches.

References

1. X. Yu and O. Kaynak, "Sliding-mode control with soft computing: A survey," *IEEE Trans. Industr. Electron*. 56(9), 3275–3285 (2009), doi: 10.1109/TIE.2009.2027531.
2. Y. Liu and R. Bucknall, "A survey of formation control and motion planning of multiple unmanned vehicles," *Robotica* 36(7), 1019–1047 (2018). doi: 10.1017/S0263574718000218.

https://doi.org/10.1017/S0263574719000262 Published online by Cambridge University Press

3. R. Cui, L. Chen, C. Yang and M. Chen, "Extended state observer-based integral sliding mode control for an underwater robot with unknown disturbances and uncertain nonlinearities," *IEEE Trans. Industr. Electron.* 64(8), 6785–6795 (2017), doi: 10.1109/TIE.2017.2694410.
4. R. Cui, X. Zhang and D. Cui, "Adaptive sliding-mode attitude control for autonomous underwater vehicles with input nonlinearities," *Ocean Eng.* 123, 45–54 (2016), doi: 10.1016/j.oceaneng.2016.06.041.
5. R. Cui, C. Yang, Y. Li and S. Sharma, "Adaptive neural network control of AUVs with control input nonlinearities using reinforcement learning," *IEEE Trans. Syst. Man Cybern. Syst.* 47(6), 1019–1029 (2017), doi: 10.1109/TSMC.2016.2645699.
6. J. Petrich and D. J. Stilwell, "Robust control for an autonomous underwater vehicle that suppresses pitch and yaw coupling," *Ocean Eng.* 38(1), 197–204 (2011), doi: 10.1016/j.oceaneng.2010.10.007.
7. S. B. Gibson and D. J. Stilwell, "An H∞ Loop-shaping Design Procedure for Attitude Control of an AUV," *Proceedings of the Oceans 2016 MTS/IEEE Monterey* (2016) pp. 1–7, doi: 10.1109/oceans.2016.7761167.
8. D. A. Spencer and Y. Wang, "SLQR Suboptimal Human-robot Collaborative Guidance and Navigation for Autonomous Underwater Vehicles," *American Control Conference (ACC)* (2015) pp. 2131–2136, doi: 10.1109/acc.2015.7171048.
9. M. G. Joo and Z. Qu, "An autonomous underwater vehicle as an underwater glider and its depth control," *Int. J. Control Autom. Syst.* 13(5), 1212–1220 (2015), doi: 10.1007/s12555-014-0252-8.
10. P. Sarhadi, A. Ranjbar Noei and A. Khosravi, "Model reference adaptive PID control with anti-windup compensator for an autonomous underwater vehicle," *Robot. Auton. Syst.* 83, 87–93 (2016), doi: 10.1016/j.robot.2016.05.016.
11. X. Huang, Y. Li, F. Du and S. Jin, "Horizontal path following for underactuated AUV based on dynamic circle guidance," *Robotica* 35(4), 876–891 (2017), doi: 10.1017/S0263574715000867.
12. A. Lari and A. Khosravi, "An evolutionary approach to design practical μ synthesis controllers," *Int. J. Control Autom. Syst.* 11(1), 167–174 (2013), doi: 10.1007/s12555-012-0181-3.
13. S. Mahapatra and B. Subudhi, "Design and experimental realization of a backstepping nonlinear H∞ control for an autonomous underwater vehicle using a nonlinear matrix inequality approach," *Trans. Inst. Measur. Control.* 40(11), 3390–3403 (2017). doi: 10.1177/0142331217721315.
14. F. Rezazadegan, K. Shojaei, F. Sheikholeslam and A. Chatraei, "A novel approach to 6-DOF adaptive trajectory tracking control of an AUV in the presence of parameter uncertainties," *Ocean Eng.* 107, 246–258 (2015), doi: 10.1016/j.oceaneng.2015.07.040.
15. V. Utkin, "Variable structure systems with sliding modes," *IEEE Trans. Autom. Control.* 22(2), 212–222 (1977), doi: 10.1109/tac.1977.1101446.
16. D. Yoerger and J. Slotine, "Robust trajectory control of underwater vehicles," *Oceanic Eng.* 10(4), 462–470 (1985), doi: 10.1109/joe.1985.1145131.
17. C. Vuilmet, "High Order Sliding Mode Control Applied to a Heavyweight Torpedo," *Proceedings of 2005 IEEE Conference on Control Applications*, 61–66 (2005), doi: 10.1109/cca.2005.1507101.
18. P. Ghiglino, J. L. Forshaw and V. J. Lappas, "Online evolutionary swarm algorithm for self-tuning unmanned flight control laws," *J. Guid. Control Dynam.* 38(4), 772–782 (2015), doi: 10.2514/1.g000376.
19. P. Poksawat, L. Wang and A. Mohamed, "Automatic tuning of attitude control system for fixed-wing unmanned aerial vehicles," *IET Control Theory Appl.* 10(17), 2233–2242 (2016), doi: 10.1049/iet-cta.2016.0236.
20. S. Khoshnam, "Three-dimensional tracking control of autonomous underwater vehicles with limited torque and without velocity sensors," *Robotica*, 36(3), 374–394 (2017), doi: 10.1017/S0263574717000455.
21. P. Poksawat, L. Wang and A. Mohamed, "Gain scheduled attitude control of fixed-wing UAV with automatic controller tuning," *IEEE Trans. Control Syst. Technol.* 99, 1–12 (2017), doi: 10.1109/tcst.2017.2709274.
22. D. C. Fernandez and G. A. Hollinger, "Model predictive control for underwater robots in ocean waves," *IEEE Robot. Autom. Lett.* 2(1), 88–95 (2017), doi: 10.1109/lra.2016.2531792.
23. M. P. Aghababa, "3D path planning for underwater vehicles using five evolutionary optimization algorithms avoiding static and energetic obstacles," *Appl. Ocean Res.* 38, 48–62 (2012), doi: 10.1016/j.apor.2012.06.002.
24. S. M. Zadeh, A. M. Yazdani, K. Sammut and D. M. W. Powers, "Online path planning for AUV rendezvous in dynamic cluttered undersea environment using evolutionary algorithms," *Appl. Soft Comput.* 70, 929–945 (2018). doi: 10.1016/j.asoc.2017.10.025.
25. S. Bing, Z. Daqi and Y. Simon, "Real-time hybrid design of tracking control and obstacles avoidance for underactuated underwater vehicles," *J. Intell. Fuzzy Syst.* 30(5), 2541–2553 (2016), doi: 10.3233/ifs-151799.
26. T. I. Fossen, *Marine Control Systems: Guidance, Navigation and Control of Ships, Rigs and Underwater Vehicles* (Marine Cybernetics AS, Trondheim, Norway, 2002).
27. E. Taheri, Kinodynamic Path Planning for Autonomous Underwater Vehicle *Ph.D Thesis* (Electrical Engineering Malek-Ashtar University of Technology, 2018).
28. I. E. Makrini, C. R. Guerrero and D. Lefeber, "The variable boundary layer sliding mode control: A safe and performant control for compliant joint manipulators," *IEEE Robot. Autom. Lett.* 2(1), 187–192 (2017), doi: 10.1109/lra.2016.2587059.
29. X. Zhang and F. Guo, "Sliding mode-like fuzzy logic control with boundary layer self-tuning for discrete nonlinear systems," *Found. Appl. Intell. System.* 213, 479–490 (2013), doi: 10.1007/978-3-642-37829-4_41.

30. H. Seok, K. Yongho, L. C. Hyun, H. Lee and M. Park, "Design of sliding-mode control based on fuzzy disturbance observer for minimization of switching gain and chattering," *Soft Comput.* 19(4), 851–858 (2015), doi: 10.1007/s00500-014-1412-8.
31. C. Yu, X. Xiang, P. Wilson and Q. Zhang. "Guidance-error-based robust fuzzy adaptive control for bottom following of a flight-style AUV with delayed and saturated control surfaces," *IEEE Trans. Cybern.* (2018).

Appendix

The numerical values of the AUV simulation parameters are listed here.

Parameter	Description	Value	Parameter	Description	Value
a_{11}	System matrix component	−0.3405	M_{uq}	Added mass cross-term and fin lift	−5.22
a_{12}	System matrix component	−0.4950	Z_{uq}	Added mass cross-term and fin lift	−9.23
a_{21}	System matrix component	−1.9650	M_{uw}	Body and fin lift	31.2
a_{22}	System matrix component	−0.2095	N_{uw}	Body and fin lift	−31.2
b_{11}	Input matrix component	0.3591	Y_{uv}	Body lift force and fin lift	−17.321
b_{21}	Input matrix component	−1.3255	Z_{uw}	Body lift force and fin lift	−17.321
X_g	Center of mass	0.0 mm	I_{XX}	Moments of inertia	38.93 Kg m^2
Y_g	Center of mass	0.0 mm	I_{YY}	Moments of inertia	37571 Kg m^2
Z_g	Center of mass	30 mm	I_{ZZ}	Moments of inertia	37571 Kg m^2
X_b	Center of buoyancy	0.0 mm	X_{prop}	Propeller thrust	5.12 N
Y_b	Center of buoyancy	0.0 mm	K_{prop}	Propeller torque	0.0 N m
Z_b	Center of buoyancy	0.0 mm	u	Surge speed	1.534 $m/sec.$

https://doi.org/10.1017/S0263574719000262 Published online by Cambridge University Press